Stellar collisions in young star clusters

Gaburov, E.

Publication date
2008

Chapter 4

Dynamics of the first collision in young star clusters

Based on:
E. Gaburov, A. Gualandris and S. Portegies Zwart
Monthly Notices of the Royal Astronomical Society, 384, 376, 2008

ABSTRACT

We study the circumstances under which the first collision occurs in young and dense star clusters. The initial conditions for our direct N-body simulations are chosen such that the clusters experience core collapse within a few million years, before the most massive stars have left the main-sequence. It turns out that the first collision is typically driven by the most massive stars in the cluster. Upon arrival in the cluster core, by dynamical friction, massive stars tend to form binaries. The enhanced cross section of the binary compared to a single star causes other stars to engage the binary. A collision between one of the binary components and the incoming third star is then mediated by the encounters between the binary and other cluster members. Due to the geometry of the binary-single star engagement the relative velocity at the moment of impact is substantially different than in a two-body encounter. This may have profound consequences for the further evolution of the collision product.

4.1 Introduction

In recent years, it became clear that stellar collisions are common events in young dense star clusters, and that such events are natural ways to form stellar exotica. In extreme cases, it is even possible that a large number of stars merge to form a very massive object. This object can potentially be a progenitor of an intermediate mass black hole.

Portegies Zwart et al. (1999) carried out the first N-body simulations of runaway stellar collisions. In these simulations, a very massive object forms in a young dense star cluster in just a few million years. It was found that the collision rate is roughly an order of magnitude greater than one would naively expect from collision cross-section arguments. The cause of the discrepancy is mass segregation, which enhances the central region with massive stars. Once in the core, these stars dominate the collision rate because of their large masses and radii. Since a collision occurs preferentially between two massive stars, the collision product becomes one of the most massive objects in the central region. If conditions are right, the product can experience multiple collisions, each time increasing its mass. This process can lead to the formation of a very massive object. The evolution of very massive stars and of collision products is not yet well understood, but one may speculate that these massive objects evolve into intermediate mass black holes.

Numerical simulations carried out by Portegies Zwart et al. (2004) show that the onset of a runaway merger depends on both the dynamical friction timescale and the central concentration of the star cluster. In particular, a necessary condition for the runaway collision to proceed is the dynamical friction timescale to be smaller than the lifetime of massive stars, which is about a few million years. If this condition is not satisfied, the mass loss due to supernovae causes the cluster to expand, and this prevents the cluster from developing the high densities required for subsequent collisions.

In their work, Gürkan et al. (2004) carried out systematic studies of mass segregation and core collapse in dense star clusters. They found that moderately concentrated star clusters with a realistic initial mass function can reach the runaway phase before massive stars produce supernovae. The runaway phase was also studied by Freitag et al. (2006), who found that the mass function of colliding stars is bimodal. The first peak lies in the lower limit of the initial mass function, 0.1 - 1$M_\odot$, whereas the second peak is close to the high-mass end of the initial mass function, 40-120$M_\odot$. They also found that collisions occur every few ten thousand years, which is roughly the time required for a collision product to reach the main-sequence.

Stellar collisions also play an important role in the formation of stellar exotica in young star clusters, such as blue stragglers. If cluster properties are such that the runaway phase is not possible, stellar collisions might still occur in the cluster producing massive bright stars. Such stars might easily

be misclassified during observations. A possible example of these stars is provided by the Pistol star in the Quintuplet cluster (Figer et al., 1998a), which is thought to have an initial mass in excess of two hundred solar masses. The lifetime of such a star is roughly three million years. However, the cluster population is about six million years old, significantly older than the Pistol star. It is therefore possible that the Pistol star is in fact an ejected collision product instead of a primordial very massive star.

In this work, we study the dynamics of the first stellar collision in young star clusters. The aim is to find a set of appropriate initial conditions for subsequent hydrodynamic simulations of collision products. In particular, we focus on the conditions under which the first collision takes place in a cluster, like the time and place of the first collision, the number of stars and binaries involved, the masses of the participating stars, the orbital parameters of the binaries, the typical impact parameter and relative velocity in the collision. The knowledge of the dynamical properties of stellar collisions will allow us to perform hydrodynamic simulations of mergers. The study of the evolution of merger products determines the observational properties of these objects, thus providing valuable information for their identification. Once the main characteristics of the evolution of collision remnants will be understood, we will proceed with the study of the dynamics of repeated stellar collisions in star clusters, with the aim to answer the question of whether a runaway process can result in the formation of a very massive object, which in turn may evolve into an intermediate mass black hole.

This chapter is organised as follows. In Sect. 4.2 we present initial conditions for our simulations. The detailed studies and the geometry of the first collision is presented in Sect. 4.3 and Sect. 4.4. A discussion of results is presented in Sect. 4.5.

4.2 Setup and initial conditions

In order to study the onset of the first collision, we focus on young star clusters with different initial virial radii ($R_{\rm vir}$) which we vary over more than one order of magnitude, while maintaining the total mass of the cluster constant. The choice of keeping $R_{\rm vir}$ as a free parameter is motivated by the aim to study the dependence of the moment of the first collision on the cluster size. Clusters with similar initial conditions but different sizes exhibit homologous evolution as far as non-dynamical processes, like stellar and binary evolution, are not of significant importance. However, in the case of stellar collisions individual stellar radii play a crucial role. In this case, the evolution of the star cluster in principle is not homologous; in other words, the two stars which collide in one case will not necessary collide if the cluster size is changed. The reason is that by scaling the cluster in size, the stellar radii relative to the cluster size also changes. By varying $R_{\rm vir}$ we

Model	$R_{\rm vir}$ [pc]	$N_{\rm run}$	$r_{\rm core}$[pc]	$\rho_{\rm core}$ [$M_\odot$/pc^3]	$t_{\rm cross}$[kyr]	$t_{\rm rlx}$[Myr]
W9R05	0.05	100	$3.2 \cdot 10^{-3}$	$5.5 \cdot 10^{9}$	1.5	0.47
W9R10	0.10	100	$6.4 \cdot 10^{-3}$	$6.8 \cdot 10^{8}$	4.3	1.4
W9R25	0.23	100	0.015	$5.6 \cdot 10^{7}$	15	4.7
W9R50	0.50	99	0.032	$5.5 \cdot 10^{6}$	48	15
W9R75	0.75	110	0.048	$1.6 \cdot 10^{6}$	88	28

Table 4.1: *Parameters of the five sets of simulations. In each case the total mass of the cluster is $M \simeq 1.2 \times 10^4\,M_\odot$ and the total number of stars is 24576. Runs differ only in the choice of the half-mass radius. In the first three columns we report the name of the set of simulations, the virial radius (in parsec) and the number of simulations performed with these parameters. In the subsequent columns we give the initial core radius (in parsec), the initial core density (in solar masses per cubic parsec), the half-mass crossing time (in units of 1000 years) and the relaxation time (in Myr).*

will be able to determine its influence on the collisions in star clusters.

All our calculations are performed using the `kira` integrator from the `starlab` gravitational N-body environment (Portegies Zwart et al. (2001))[1]. Stellar evolution in the simulations is included via the `SeBa` package Portegies Zwart & Verbunt (1996). Binaries, though initially not present, form dynamically in the course of the simulations and are evolved using `SeBa`. All N-body simulations were carried out on the MoDeStA[2] cluster of GRAPE-6 (Makino et al., 2003, 1997) in Amsterdam.

We present the initial conditions for the different sets of simulations in Tab. 4.1. Each simulation is carried out with N=24576 single stars distributed in a King (1966) model with a scaled central potential $W_0 = 9$ (Binney & Tremaine, 1987). We did not include primordial binaries because we aim to study large parameter space in this work.

Such a choice of W_0 is motivated by our interest in studying young star clusters such as R136, MGG11 and Arches (Massey & Hunter, 1998; Figer et al., 2002; McCrady et al., 2005), and young star clusters are thought to be born with high concentration (Merritt et al., 2004b). In addition, high concentration is a necessary condition for clusters which can experience runaway stellar mergers (Portegies Zwart et al., 2004). As we are interested in the internal dynamics, the effect of the tidal fields is expected to be negligible (Portegies Zwart et al., 2007b); therefore, our simulations are carried out without tidal fields. After generating stellar positions and velocities, we assign masses to each of the stars from an initial mass function(Kroupa et al. (1993); Kroupa (2001)) between $0.1\,M_\odot$ and $100\,M_\odot$, which we refer to as IMF. We subsequently scale the velocities of all stars to bring the cluster into virial equilibrium. Such initial conditions produce star clusters with a

[1] `http://www.manybody.org/starlab`

[2] `http://modesta.science.uva.nl`

total mass of roughly $10^4 M_\odot$, which approximates well the Arches cluster (Figer et al., 1999, 2002).

For each set of initial conditions with $W_0 = 9$, we generate about a hundred realisations, each of which we run until the first collision occurs. We identify a collision in our simulations when two stars pass each other within a distance smaller than the sum of their radii; tidal captures are ignored. The binary evolution package allows for semi-detached and contact binaries to transfer mass. In our analysis, we discriminate between two types of collisions: those that result from unstable mass transfer in a close binary system and those that result from a dynamical interaction. The latter case we identify as a collision, whereas the former case is referred to as coalescence. In this work we focus on physical collisions between stars.

Our code employs "standard N-body units"[3] (Heggie & Mathieu (1986)), according to which the gravitational constant, the total mass and the radius of the system are taken to be unity. The resulting unit of time is the N-body time-unit and is related to the physical crossing time of the system through the relation $T_{\rm cross} = 2\sqrt{2}\, t_{\rm Nb}$.

4.3 The circumstances of the first collision

In order to develop a better understanding of stellar collisions and of the further evolution of the collision product, it is important to know the conditions under which a collision takes place, such as the mass, structure and composition of the participating stars, and the geometry under which the collision occurs.

4.3.1 The location of the first collision

Since the stellar density is highest in the cluster core, we expect that majority of collisions to take place in the central region. In the top panel of Fig. 4.1, we show the distribution of the number of collisions as a function of the distance to the cluster centre. All simulations presented in Tab. 4.1 are included in the sample. Out of a total of 282 collision in 509 simulations, only 33 occur outside the instantaneous core of the cluster.

Though a small fraction (12 %), it is interesting that a sizeable number of collisions occurs outside the core of a cluster. This can be naturally explained as follows. In a cluster with a density profile $\rho(r)$, the expected number of collisions in a spherical shell located at radius r is $N \propto r^2 \rho(r)^2$, and therefore one may expect a small, but finite, number of collisions to occur just outside the core. To test this, we fitted this expression to the number of collisions. As a density profile, we used a variety of King models with different values of W_0. We found that King models with $W_0 \gtrsim 9$ fit

[3] `http://en.wikipedia.org/wiki/Natural_units#N-body_units`.

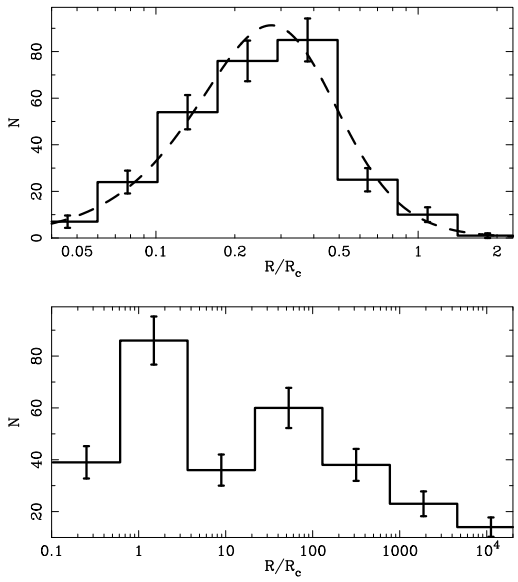

Figure 4.1: *Histogram of the number of collisions in all simulations as a function of the distance to the cluster centre in units of the instantaneous core radius. In the upper panel, the dashed line displays the fitted model of the number of collision. In the lower panel we present the distribution of coalescence as a function of distance to the centre of a cluster.*

well ($\chi^2 \approx 1$) since their density profiles in the close neighbourhood of the core are essentially the same.

In the lower panel we present the distribution of number of coalescence as a function of the distance to the cluster centre. We see that the coalescence can occur quite far from the core of the cluster; such coalescence are ejected binary stars in which the massive companion leaves the main-sequence. The number of coalescence events far away from the core decreases as a function of distance to the cluster centre.

4.3.2 The time of the first collision

In Fig. 4.2, we show the time distributions for the formation of the first hard binary and for the first collision. The first collision occurs preferentially after the formation of the first hard binary, but the distribution is broad and extends all the way to $\sim 200N$-body time units. We notice that the coalescence dominate at $t \gtrsim 20$ N-body units, whereas collisions are dominant earlier.

The evolution of the mass function in the cluster centre is mainly driven by dynamical friction, which preferentially brings massive stars to the core. As a result, the mass function in the core becomes flatter with time, and after core collapse the mass function stops evolving except for the effects of

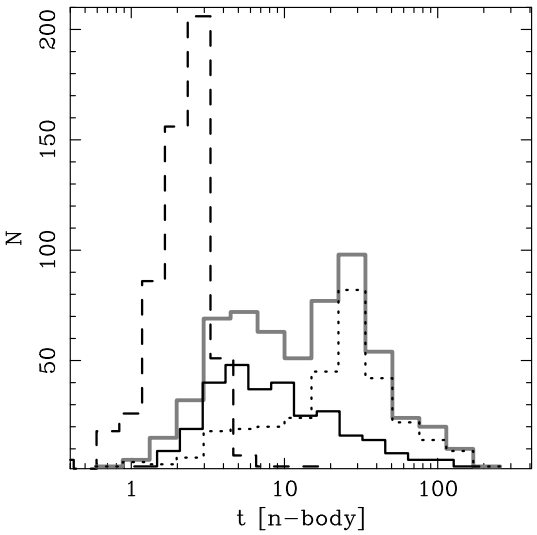

Figure 4.2: *Histogram of the number of first $|E| > 100\,kT$ binaries (dashed line), first collisions (solid line) or first coalescence (dotted line) as a function of time (expressed in N-body units). The total number of mergers (collisions + coalescence) in a time-bin is shown with a thick gray solid line.*

stellar evolution, such as decrease of the number of massive stars in a star cluster (Portegies Zwart et al., 2007b).

In Fig. 4.3 we present mass functions in the core at the moment of the first collision averaged over all simulations in which a collision happens. The mass functions for different models are consistent with a single distribution better than at a 25% level. However, for models W9R50 and W9R75 the consistency is less than at 5% level, which is due to the effects of stellar evolution. As the ratio of a stellar evolution timescale to a dynamical timescale is inversely proportional size of a star cluster, the effects of stellar evolution become increasingly important as the size of the cluster increases. While stellar evolution does not have a notable influence on models W9R05, W9R10 and W9R25, it clearly leaves an imprint in models W9R50 and W9R75 (see also Appendix 4.A).

The mass function in the core after the first collision can be approximated by the following expression:

$$\mathcal{N}_{\rm c}(m) \propto \begin{cases} \mathcal{N}_{\rm IMF}(m), & \text{if } m < m_1 = 2\langle m_{\rm IMF}\rangle, \\ m\,\mathcal{N}_{\rm IMF}(m), & \text{otherwise.} \end{cases} \tag{4.1}$$

Here $\mathcal{N}_{\rm IMF}(m)$ is the initial mass function and $\langle m_{\rm IMF}\rangle$ is the average mass of the initial mass function. This expression is presented as the thick solid line in Fig. 4.3. Equation 4.1 implies that for stars more massive than $\sim 2\langle m_{\rm IMF}\rangle$ the slope of the mass function flattens. This is not unexpected since the dynamical friction time-scale is inversely proportional to m. We

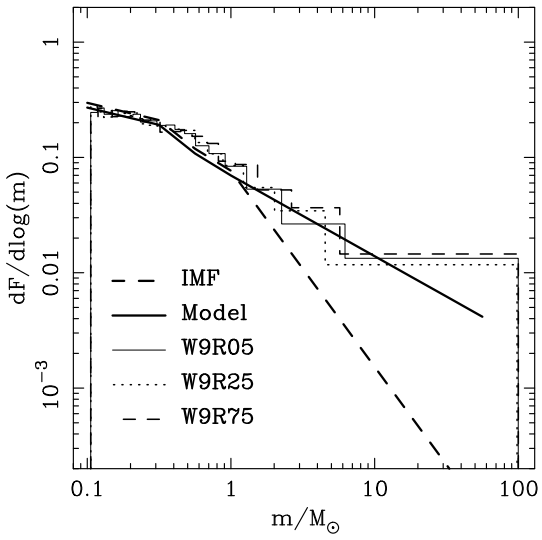

Figure 4.3: *Mass function in the core at the moment of the first collision averaged over all runs for each model. The thick dashed line represents the IMF whereas the thick solid line represents Eq. 4.1 which satisfactory represents the simulated mass function in the core.*

conclude that dynamical friction is a crucial ingredient in understanding the first collision.

In Fig. 4.4 we compare the time of the first collision, $t_{\rm coll}$, with the time-scale on which a star with mass m sinks to the cluster centre from its initial orbit, $t_{\rm decay}$.

We compute $t_{\rm decay}$ for the most massive star that participates in the first collision by integrating its equations of motion from the initial orbit until the star decays to the cluster centre. We include the effect of dynamical friction using $\log(\Lambda) = \max(0, \log(0.4M_{\rm cl}(r)/m))$, where $M_{\rm cl}(r)$ is the cluster mass enclosed within a sphere of radius r (Binney & Tremaine, 1987). As for the background potential, we adopt a King $W_0 = 9$ density profile which represents our initial simulation model.

The correlation between $t_{\rm coll}$, which is taken directly from the simulations, and $t_{\rm decay}$, which is calculated as described above, is presented in Fig. 4.4. In the left panel the results are given in units of the core collapse time as measured in the simulation under consideration, whereas in the right panel time is given in physical units.

In the left panel of Fig. 4.4 we identify three different regimes. The majority of collisions are distributed along $t_{\rm coll} = t_{\rm decay}$ (area 1 in Fig. 4.4). This indicates, as we suggested earlier, that dynamical friction is dominant in determining the moment of the first collision. A collision occurs quickly upon the arrival of the star in the core.

The dispersion along $t_{\rm decay}$ in area 1 of Fig. 4.4 is in part a consequence

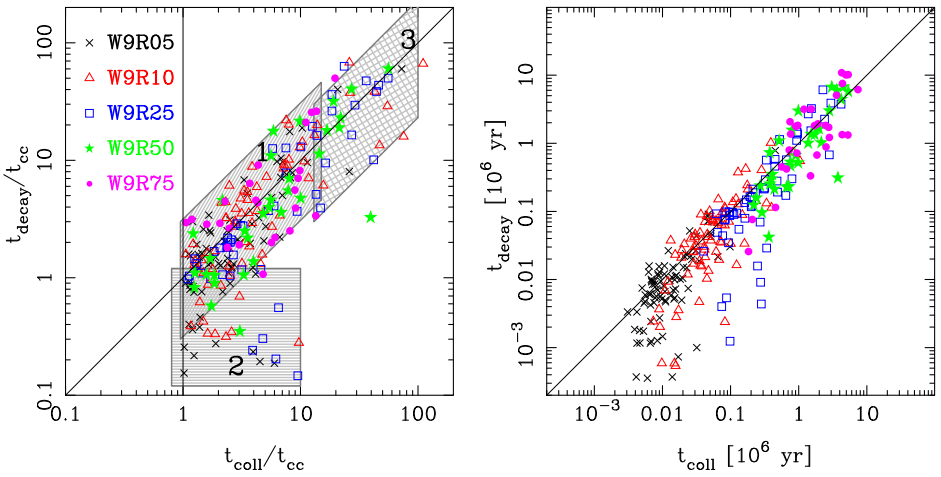

Figure 4.4: *Correlation between* $t_{\rm coll}$ *and* $t_{\rm decay}$ *. In the left panel* $t_{\rm coll}$ *and* $t_{\rm decay}$ *are given in N-body units while in the right panel they are in physical units. The results from different models are indicated with different symbols and colours. The diagonal in both panels gives the line for which* $t_{\rm coll} = t_{\rm decay}$ *. The gray shaded areas in the left panel, numbered 1, 2 and 3, indicate three different regimes, as described in the text.*

of our assumption that the background potential is static throughout our calculations of $t_{\rm decay}$. The density profile of the clusters, however, is calculated self consistently in our N-body simulations, and it changes with time. In addition, even when the star arrives in the core, it still takes some time before it engages in a collision. The latter effect is visible in area 2 of Fig. 4.4.

In area 2 of Fig. 4.4, we present the stars that experience a collision later than one would naively expect from their calculated decay time. These stars are born in or near the cluster centre but a collision is delayed up to the moment of core collapse. After that, the stars still have to participate in a strong encounter which leads to a collision. Thus, the moment of the collision is determined by $t_{\rm cc}$ and the time required to find a suitable collision candidate, and this may take up to about $10\,t_{\rm cc}$.

It is somewhat surprising that there is a third region along the line $t_{\rm coll} = t_{\rm decay}$, which is illustrated in the area 3 of Fig. 4.4, and which extends all the way to $t_{\rm coll} \simeq 100\,t_{\rm cc}$. As a rule of thumb, it takes roughly 50 N-body units for a $50{\rm M}_\odot$ star to decay from the half-mass radius to the core. From area 2, it can be seen that a star in the core may require up to $10\,t_{\rm cc}$, which roughly corresponds to 30 N-body time units (see Fig. 4.2), to engage in a collision. Since we expect our simulations to host at least one $50{\rm M}_\odot$ star which is initially located within the half-mass radius, it is rather unlikely to have collisions in our simulations after $t \simeq 15 t_{\rm cc}$; still, some collisions do

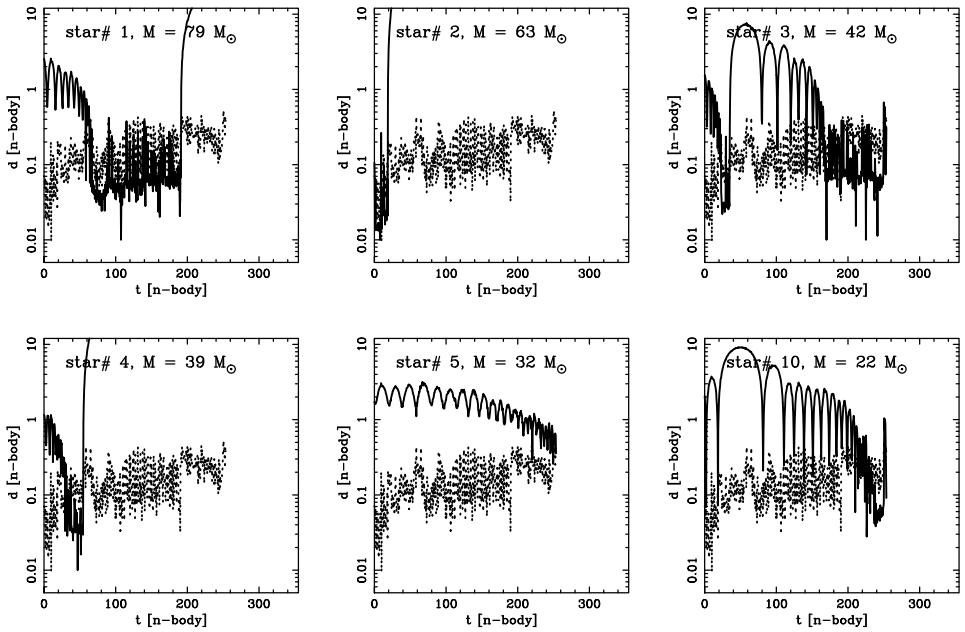

Figure 4.5: *Distance to the cluster centre for six of the most massive stars in one of the simulations from model W9R05. The dotted curve in each panel gives the evolution of the core radius of the model (which is identical in each panel). The solid curve gives the evolution of the distance to the cluster centre for the star identified in the top left corner of the panel.*

happen as late as $100\,t_{\rm cc}$.

These late collisions, which are illustrated in area 3 of Fig. 4.4, are attributed to massive stars that reach the core but instead of experiencing a collision are ejected from the cluster in a strong encounter with a binary. This effectively delays the moment of the first collision since the potential target star is removed from the cluster. If this happens, the first collision is postponed until the moment when another massive star reaches the cluster core and subsequently collides. In Appendix 4.B we show that such self-ejections are possible in clusters with mass

$$M_{\rm cl} \gtrsim 2 \cdot 10^4 \left(\frac{m_\star}{50\,{\rm M}_\odot}\right)^3 \left(\frac{m_{\rm s}}{10{\rm M}_\odot}\right)^{-2} {\rm M}_\odot. \qquad (4.2)$$

Here, $m_\star$ is the mass of an ejected star, and $m_{\rm s}$ is the mass of the star triggering the ejection event.

The process described in the previous paragraph is illustrated in Fig. 4.5 where we present the evolution of the distance to the cluster centre for several of the most massive stars in one of the simulations of W9R05 (see Tab. 4.1). In addition, we plot the evolution of the core radius in each panel.

The most massive cluster member, star #1 of $79{\rm M}_\odot$, which is presented

in the top left panel of Fig. 4.5, sinks from about the half-mass radius to the cluster core in roughly 50 N-body time units ($\simeq 15 t_{\rm cc}$in this particular run). It becomes a binary member at $t \simeq 88.5$ and the binary increases its binding energy to $\sim 100\,$kT at $t \simeq 165$ N-body time units. Star #1 stays in the core until it is ejected at about 200 N-body time units, never to return again. Even though star #1 is the most massive star in the system, it is part of a binary system and it resides in the cluster centre for more than $100N$-body time units, it does not participate in a collision but is ejected from the core.

The same process causes several of the other massive stars to be ejected, such as stars #2 and #4 in Fig. 4.5, whereas some of the other massive stars, such as stars #3 and #5, are not ejected. These repeated ejections of high-mass stars delay the collision until nearly 250 N-body time units, which roughly corresponds to 80 $t_{\rm cc}$. Eventually, it is $22 {\rm M}_\odot$star #10 which reaches the core and experiences a collision with a $4 {\rm M}_\odot$ star.

4.3.3 Mass distributions

The binary which forms during core collapse is likely to be the candidate for a collision. However, this does not mean that the two stars in the binary coalesce, instead this enhances the probability for a collision with a third star.

In Tab. 4.2 we present the number of collisions that occurred in each of the models with respect to the choreography of the triple interaction. The notation is as follows: the two binary members are called M_p and M_s for the most massive (primary) and least massive (secondary) star respectively, while the third star is called the bullet and is indicated with M_b; the two colliding stars are presented in braces while the entire triple interaction is in parenthesis.

The collisions in the densest star clusters (model W9R05 and W9R10) are dominated by collisions between the primary and the bullet star. The fraction of these collisions remains roughly constant compared to the total number of collisions. The shallowest clusters (model W9R50 and W9R75), on the other hand, are governed by binary evolution, which does not come as a surprise since stellar evolution plays an increasingly important role as the size of the cluster increases. In some cases, however, the primary is not participating in the collision, but instead it is the secondary star that collides with the bullet.

In the left panel of Fig. 4.6, we present the distribution of primary masses. These distributions are statistically indistinguishable for the three densest clusters (models W9R05, W9R10 and W9R25), whereas for the shallowest clusters (models W9R50 and W9R75) they deviate in that the mean mass for the primary stars decreases. This is the result of stellar evolution, which becomes gradually more important for shallower clusters. The mass

Model	$(\{M_p, M_b\}, M_c)$	$(\{M_s, M_b\}, M_p)$	$(\{M_p, M_s\}, M_b)$	$N_{\rm c}$	$N_{\rm m}$
W9R05	67	15	5	87	13
W9R10	59	11	9	79	21
W9R25	37	12	5	54	46
W9R50	16	12	5	33	66
W9R75	19	5	5	29	81

Table 4.2: *The choreography of triple interactions leading to a collision in the different calculations. In the first column, we present the model name followed by the number of collisions in each of the configurations. These are: a collision between the primary and the bullet (column two), a collision between the secondary and the bullet (column three) and a collision between the primary and the secondary star (column four). The fifth column shows the total number of collisions that are outcomes of a dynamical interaction, whereas the last column shows the number of binary mergers which result from an unstable phase of mass transfer in a dynamically formed binary. The latter category is not further discussed in this work.*

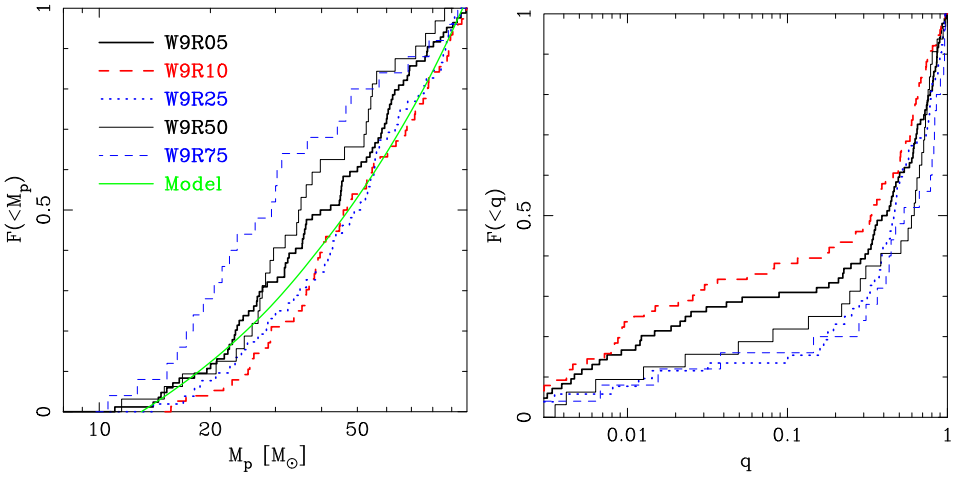

Figure 4.6: *Distribution of primary masses (left) and mass ratios (right) for binaries participating in the collision. According to Kolmogorov-Smirnov test there is 15%, 28%, 90%, 5% and 0.2% chance for models W9R05, W9R10, W9R25, W9R50 and W9R75 respectively that the deviations in the distributions from the theoretical curve are random in nature. The green solid line is a cumulative mass function in the core (Appendix 4.A), but with the lower mass limit taken to be* $15\mathrm{M}_\odot$.

functions of the primary in models W9R05, W9R10 and W9R25 are consistent with the mass function in the core at the moment of the first collision (Appendix 4.A), if only stars above $15\,\mathrm{M}_\odot$ are taken into account.

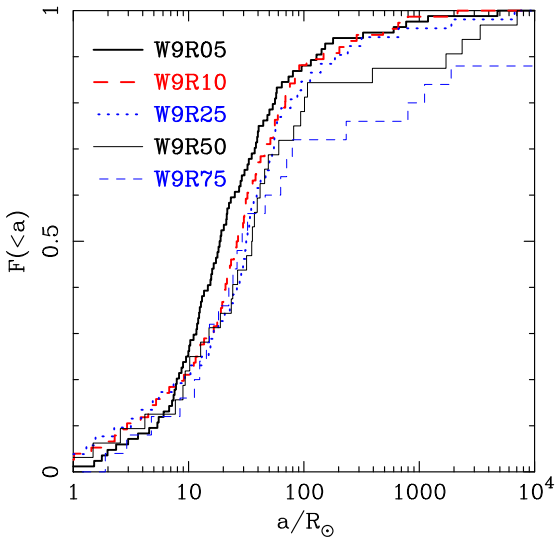

Figure 4.7: *Distribution of semi-major axes for binaries undergoing a collision. Binaries with separation smaller than the sum of their stellar radii $a \lesssim 10\,\mathrm{R}_\odot$ are contact binaries which form in the course of the simulation.*

In the right panel of Fig. 4.6, we present the distribution of the mass ratio of the secondary to the primary star. Here, we see that the mass ratio for shallower clusters is systematically higher than for denser clusters. This trend we explain by the fact that the binaries in shallower clusters experience more interactions before they participate in a collisions, allowing for exchanges of a more massive star into the binary. This is supported by Fig. 4.7 where we plot the distribution of orbital separations of the binaries that participate in a collision event. These distributions are statistically indistinguishable when displayed in physical units. This however implies that the binaries in the larger clusters are harder as their semi-major axis is smaller when measured in N-body units.

In Fig. 4.8 we present the distribution of the masses of bullet stars colliding with the primary. The mean mass of bullet stars increases with the size of the cluster. Together with the simulation data, we present the theoretical line which gives the results of a qualitative model for the mass of the bullet star. The low-mass end of this curve follows the mass function in the cluster core at the moment of the collision, whereas for the steeper high-mass part (above $\sim 2\langle m\rangle_{\mathrm{core}}$), we weight the probability distribution with the gravitational focusing of the bullet:

$$\mathcal{N}_{\mathrm{b}}(m_{\mathrm{b}}) \propto \begin{cases} \mathcal{N}_{\mathrm{c}}(m_{\mathrm{b}}), & \text{if } m_{\mathrm{b}} < 2\langle m\rangle_{\mathrm{core}}, \\ m_{\mathrm{b}}\,\mathcal{N}_{\mathrm{c}}(m_{\mathrm{b}}), & \text{otherwise.} \end{cases} \tag{4.3}$$

We make the distinction between the enhanced cross section (high-mass end) and the geometric cross section (low-mass tail), since we expect that

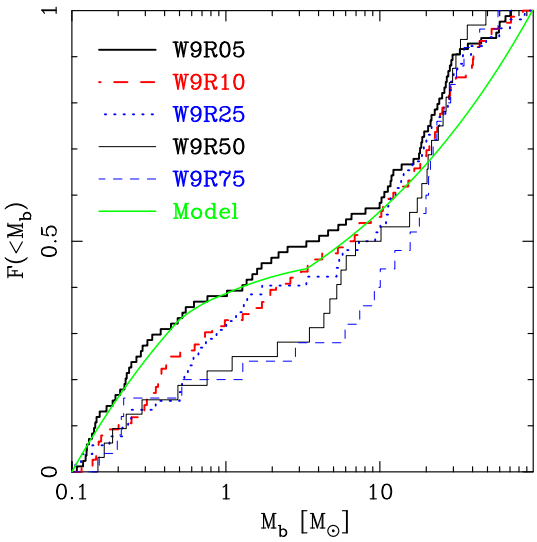

Figure 4.8: *Mass function of single stars that collide with binaries. The solid line shows a cumulative distribution function computed from a bullet mass function presented in Eq. 4.3*

for low-mass bullet stars the collision rate is dominated by the cross section of the encountering binary, rather than the bullet itself.

4.4 The collision geometry

In the previous sections, we demonstrated that all collisions in a cluster's centre occur between a binary component and a single star. This has far reaching consequences for the energetics and angular momentum of the collision. While in a two-body collision the outcome of the event depends only on the impact parameter and the relative velocity at large separation, in our simulations the situation is considerably more complicated as one of the encountering objects is always a binary member. In this case the relative velocity at the moment of the impact can be either significantly higher or lower than in the idealised two-body case. Therefore, the consequences for the evolution of the collision product may be profound.

Fig. 4.9 illustrates the two extreme cases that can occur when a bullet star collides with a star in a binary. In the left panel we show two colliding stars that are approaching each other at the moment of the first contact, whereas in the right panel we show two colliding stars that are moving in the same direction at the moment of impact, so that the binary companion is effectively receding from the bullet star.

The consequence for the impact velocity in terms of the escape speed of the merged object is illustrated in Fig. 4.10. Here, we see that about

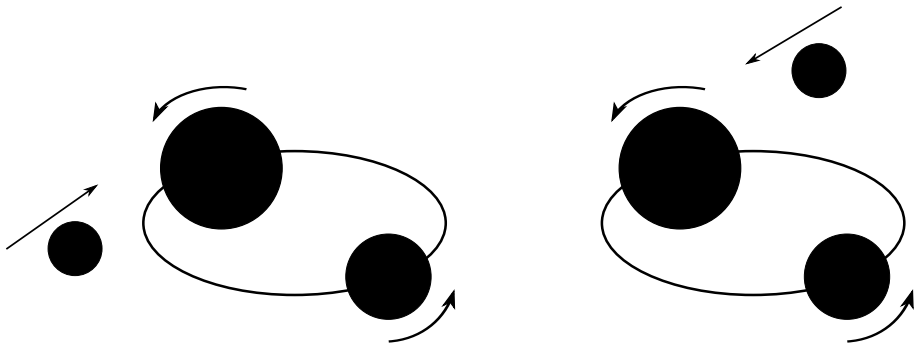

Figure 4.9: *Schematic representation of the collision between a binary member and a single star. The left figure shows the case when the two colliding stars move towards each other. In this instance, the impact velocity can exceed the escape velocity from the two body systems formed by the colliding stars. The right figure shows the case when the two interacting stars move in the same direction. In this case, if a collision occurs, the impact velocity can be smaller than the escape velocity.*

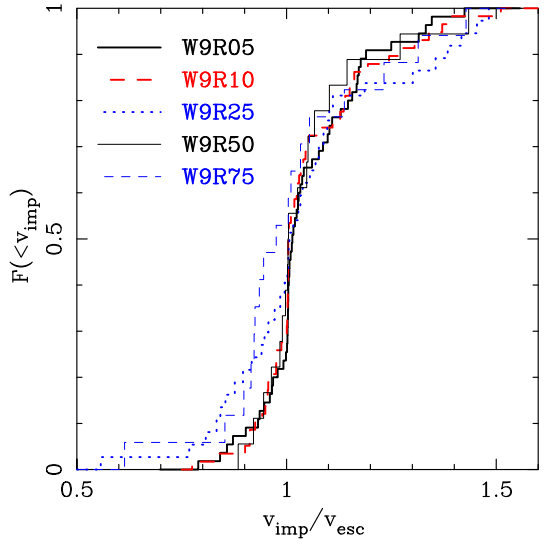

Figure 4.10: *Cumulative distribution of impact velocities in units of the escape velocity of the two-body system formed by the colliding stars. The thick solid line corresponds to a W9R05 model, the thick dashed line to a W9R10, the thick dotted line to a W9R25, the thin solid line to a W9R50 and the thin dotted line to a W9R75 model.*

half of the collisions occur with a velocity smaller than the one expected for a two-body encounter. In some extreme cases, however, the velocity at impact can be $\simeq 50\%$ higher than in the two-body case. The tail of

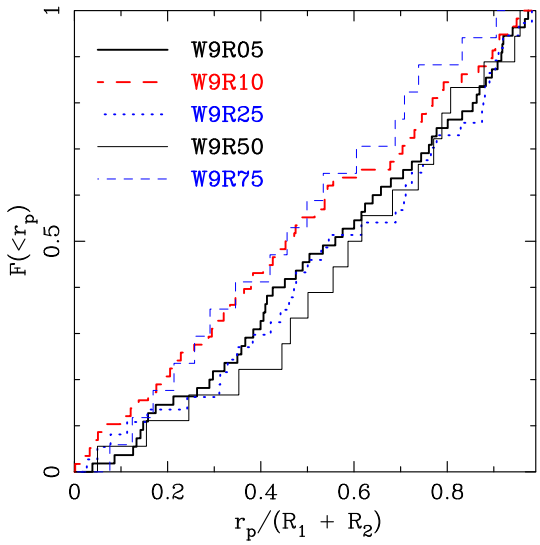

Figure 4.11: *Cumulative distribution of pericentres. The periscentres are computed assuming that two stars approach each other on a hyperbolic trajectory such that their relative velocity at contact is equal to the one observed in the simulations.*

lower impact velocities is completely absent in isolated two-body unbound encounters; this latter case is somewhat comparable to the merger of two binary components.

In Fig. 4.11, we present the distance between the two stellar centres at the moment of impact. For all models, the distribution of impact distance is flat and as a result the cumulative distribution is a straight diagonal line. This is a direct consequence of gravitational focusing, which dominates even in these three-body encounters. The chance to have a relatively small impact distance is comparable to the chance of having a very large impact distance, which is against our naive intuition that the probability of a collision $\propto R_\star^2$.

4.5 Discussion and conclusions

We have studied the dynamics of the first stellar collision occurring in the evolution of young star clusters by means of high-accuracy direct N-body simulations. We have carried out about 500 simulations of star clusters represented by King models of different central concentration and different size.

During the early evolution of young dense clusters, massive stars sink to the core due to dynamical friction. As a result, the core becomes enhanced with massive stars, which can be seen in the flattening of the core mass function for $m \gtrsim 2\langle m \rangle$. Due to the steeper dependence of the binary formation cross-section on stellar mass than the collision cross-section, binary

formation becomes a more likely process than a collision. Young clusters are, in this respect, different from globular clusters, where binary formation by three-body encounters is unimportant (Hut & Verbunt, 1983).

Collisions occur after the formation of hard binaries in the core of the cluster. As expected, nearly all collisions occur in the core of the star cluster. The time of the first collision is roughly equal to the time required for the most massive colliding star to reach the core. While most of the collisions occur within a timescale of 50 N-body time units ($15t_{\rm cc}$), we find that some of them are delayed to as much as a few hundred N-body time units. This is due to the fact that some of the massive stars that have reached the core are ejected from the cluster during dynamical encounters. This process postpones the first collision event to later times.

As for the geometry of the collision, we have found that most of the collisions occur between the primary star of a participating binary and a single star. The fraction of these collisions remains constant as the size of the cluster changes, except for the models W9R50 and W9R75 which are affected by stellar evolution. The masses of the primary star are distributed according to the core mass function but only for stars with $M_p \gtrsim 10\,{\rm M}_\odot$. The bullet stars, on the other hand, are single core stars.

One of the consequences of this geometry is that the impact velocity covers a wide range of values: from roughly 50% to 150% of the escape velocity from the two-body system formed by the two colliding stars. On the one hand, the low velocity tail of the impact velocity would be impossible if collisions were to occur between two unbound stars; however, this situation is to some degree similar to the merger of a binary. On the other hand, the high velocity tail can only occur if the dispersion velocity in the system is comparable to the escape velocity from the stellar surface. Such high velocity collisions may result in a significant mass loss or even destruction of a star (Freitag & Benz, 2005). As for the impact parameter, we have found that all collisions are dominated by gravitational focusing. The distribution of pericentre separations implies that nearly head-on collisions are as frequent as off-axis collisions.

As the collisions occur in a binary-single stellar system, there is a possibility that all stars may merge. If a single star merges with one of the binary members, the resulting collision product can expand by a large factor due to excess of thermal energy. In this case, the binary may become unstable and merge, and this therefore results in a triple merger. On the other hand, if the first encounter which involves a single star and a binary companion is not a head-on but rather grazing one, the possibly large impact velocity may prevent the merger all together. Therefore, to understand the fate of such systems one has to resort to hydrodynamic simulation.

4.A Mass function of binaries

In a given stellar population, it is possible to estimate the mass function of binary stars formed by three-body encounters. Let $\mathcal{N}(m)$ be the mass function of single stars in the region where binary formation takes place. Our aim here is to estimate the mass function of binaries formed by three-body encounters, $\mathcal{N}_{bin}(M_p, q)$. We wish to express this as a function of the mass of the primary star, M_p, which is the most massive binary companion, and the mass ratio, $q < 1$, of the secondary, which is the least massive binary companion, to the primary.

The probability to form a binary with a star of mass m_1 and another star of mass m_2 is proportional to the product of probabilities to randomly draw these stars from a mass function, $\mathcal{N}(m_1)\mathcal{N}(m_2)$, and the cross-section for these two stars to form a binary, $\Sigma(m_1, m_2)$. However, to form a binary a third star is required which carries away energy in order for m_1 and m_2 to form a bound system. In the further analysis, we assume that the mass of the third star is small compared to m_1 or m_2 and, therefore, it can be neglected in the cross-section of binary formation by three-body encounters.

Following Heggie & Hut (2003), we write the binary formation cross section in the following form

$$\Sigma(m_1, m_2)_b \propto (m_1 + m_2)/v_{12}^2. \tag{4.4}$$

Here, v_{12} is the relative velocity between two stars. Assuming energy equipartition, we write $v_{12}^2 \propto (m_1 + m_2)/(m_1 m_2)$, and Eq. 4.4 takes the following form

$$\Sigma_b(m_1, m_2) \propto m_1 m_2. \tag{4.5}$$

As we have mentioned above, the mass function of the dynamically formed binaries is

$$dF \propto dm_1 dm_2 \mathcal{N}(m_1)\mathcal{N}(m_2)\Sigma_b(m_1, m_2). \tag{4.6}$$

After the change of variables from (m_1, m_2) to $(M_p, q = M_s/M_p)$, were $M_p = \max(m_1, m_2)$ and $M_s = \min(m_1, m_2)$, this equation takes the following form

$$\frac{dF}{dq dM_p} = \mathcal{N}_{bin}(M_p, q) \propto q M_p^3 \mathcal{N}(M_p)\mathcal{N}(qM_p). \tag{4.7}$$

It is now possible to find the distribution of M_p and of q. The former can be obtained by integrating Eq. 4.7 over all possible mass ratios

$$\mathcal{N}_{bin}(M_p) = \int dq\, \mathcal{N}_{bin}(M_p, q), \tag{4.8}$$

and the latter is the integral of Eq. 4.7 over all primary masses

$$\mathcal{N}_{bin}(q) = \int dM_p\, \mathcal{N}_{bin}(M_p, q). \tag{4.9}$$

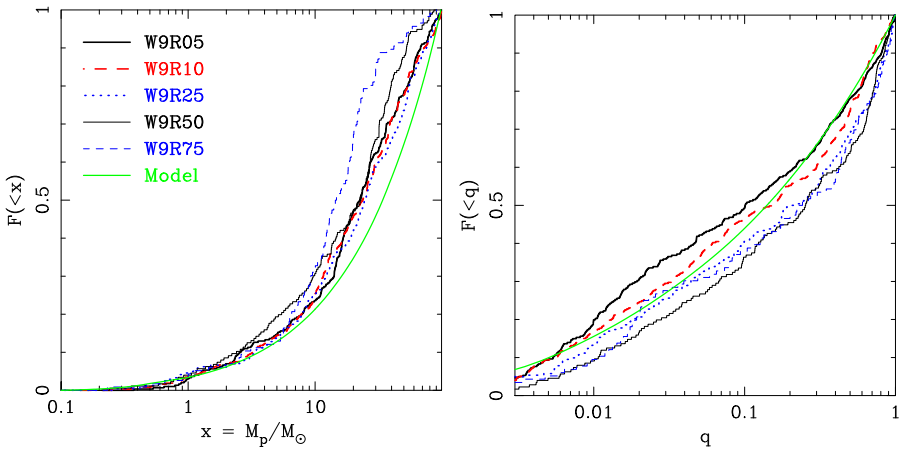

Figure 4.12: *Primary mass (left) and mass ratio (right) distribution for dynamically formed binaries. The mass distributions of primary stars for W9R05, W9R10 and W9R25 models are consistent with a single distribution function better than at 30% level. The source of the discrepancy in the high-mass end of the mass function is due to the effects of stellar evolution on the initial mass function.*

We compare both Eq. 4.8 and Eq. 4.9 with the simulations. Given the fact that most of the collisions occur in the core of a star cluster (see Sect. 4.3.2), we assume that binaries also form in the core. It was shown by Portegies Zwart et al. (2007b) that the mass function in the core is unchanged after the formation of the first hard binary. Thus, we assume that Eq. 4.1, which is the mass function at the moment of collision, is the mass function in the core of the star cluster at the moment of the formation of the first hard binary, $\mathcal{N}(m)$.

We extract the mass function of binaries which are formed by three-body encounters in the following way. For each simulation, we obtain the masses of the primary and the secondary star. Since some binaries persist for a long period of time, we make sure that the same binary is not used more than once. After that, we build distributions for the masses of the primary star and the mass ratio.

We show the resulting distributions, both from the simulations and from our semi-analytical estimates, in Fig. 4.12. It may be noted that models W9R50 and W9R75 lack massive stars. This is the result of stellar evolution that modifies the high-mass tail of the initial mass function. The effect is less pronounced in the W9R50 model and is unnoticeable in the rest of the models.

4.B Binary self-ejection

In this appendix, we estimate the minimal mass of a star cluster that can yield self-ejecting binaries.

Given a star cluster of mass M and half-mass radius R, its gravitational binding energy is

$$E \simeq \frac{GM^2}{4R}. \tag{4.10}$$

For simplicity, in this analysis we consider a binary which consists of two equal-mass stars of mass $m_\star$. The binding energy of such a binary of semi-major axis a is

$$E_b \simeq \frac{Gm_\star^2}{2a}. \tag{4.11}$$

In order to prevent a star cluster from collapse, the binary should be able to generate enough heat. In this case, we assume that the binding energy of the binary should be equal to the binding energy of the cluster. Combining Eq. 4.10 and Eq. 4.11, we show that this occurs when the semi-major axis of the binary is

$$a_{\rm eq} \simeq 2R \left(\frac{m_\star}{M} \right)^2. \tag{4.12}$$

If a single stars with mass $M_{\rm s}$ star were to interact with such a binary, it would be ejected with a velocity of the order of the orbital velocity of the members of the binary, $v_{\rm orb}^2 \simeq Gm_\star/a_{\rm eq}$. In order to conserve linear momentum, the binary itself would recoil with velocity

$$v_{\rm rec} = \frac{m_{\rm s}}{2m_\star} v_{\rm orb}. \tag{4.13}$$

Here, we assume that the mass of the low-mass star is equal to the mean stellar mass in the core, $\langle m_c \rangle$.

We estimate the escape velocity from the cluster in the following way

$$v_{\rm esc}^2 \simeq \frac{2GM}{R}. \tag{4.14}$$

Combining Eq. 4.13 and Eq. 4.14, we express the condition $v_{\rm rec} > v_{\rm esc}$ as a condition on the minimal mass of the cluster which can yield ejected binary stars

$$M \gtrsim 16 \frac{m_\star^3}{m_{\rm s}^2} \approx 2 \cdot 10^4 \left(\frac{m_\star}{50\,{\rm M}_\odot} \right)^3 \left(\frac{m_{\rm s}}{10\,{\rm M}_\odot} \right)^{-2} {\rm M}_\odot. \tag{4.15}$$